CIGRÉ - SC 38
Colloquium on Power System Dynamic Performance
Florianópolis, Brazil September 20-24, 1993

PROPOSAL FOR A BENCHMARK SYSTEM FOR POWER SYSTEM OSCILLATION ANALYSIS AND CONTROL

Nelson Martins[1] Nilo J. P. Macedo[2] André Bianco[1] Herminio J. C. P. Pinto[1] Leonardo T. G. Lima[3]

[1]CEPEL, Caixa Postal 2754, 20.001, Rio de Janeiro, RJ, Brazil - Fax Number: 55-21-260-1340
[2]FURNAS Centrais Elétricas S.A., R. Real Grandeza 219, 22.283, Rio de Janeiro, RJ, Brazil
[3]UFF/Dept. of Electrical Engineering, R. Passo da Pátria 156, 24.210, Niterói, RJ, Brazil

Abstract : *This paper proposes an AC/DC benchmark system for power system oscillation analysis and control. Detailed results are described, in a tutorial manner, utilizing several complementary methodologies for linear dynamical systems. The paper contents are control oriented including aspects such as choice of adequate feedback loops and coordinated design of multiple controllers. Adequate oscillation damping is achieved by the use of stabilizing signals, designed through frequency response techniques and added to generator excitation, HVDC links, Static VAr Compensators and other FACTS devices.*

Keywords : *small-signal stability, AC/DC power systems, electromechanical oscillations, frequency response techniques, transfer function zeros, transfer function residues, stabilizing signals, static VAr compensators, HVDC links, FACTS devices, control system design.*

1 - INTRODUCTION

Some areas of power system engineering have long adopted benchmark models to enable performance evaluation of proposed algorithms, methodologies and computer codes. There, apparently, has never been a coordinated effort to develop a benchmark system for small-signal electromechanical stability. The IEEE Working Group on System Oscillations, of the System Dynamic Performance Subcommittee, is now supporting the development of some benchmark systems. CIGRÉ has sponsored, through its Power System Dynamics Performance and Analysis Working Group (WG 38.02), several valuable contributions to the small signal stability area [1,2,3]. It has also recommended the development of powerful eigenvalue programs for the analysis of small-signal stability of large power systems [1].

The authors believe that Study Committee 38 should now have the development of benchmark systems for small-signal stability as one of its priorities.

The New England Test System [4] has naturally become a sort of benchmark for multimachine small-signal stability. This is a good reason to support the inclusion of new dynamic components (HVDC links, SVC's, FACTS devices, etc.) to obtain an updated New England benchmark.

The proposed AC/DC benchmark system of this paper has many interesting features and the advantage of being smaller than an updated version of the New England system. This paper describes detailed results, utilizing several complementary methodologies of linear dynamical systems, concerning the oscillation analysis and control of the proposed benchmark system.

Non-linear time domain simulations were not considered. The notations adopted in the paper are defined as used, except for the well established symbols.

2 - THE PROPOSED BENCHMARK SYSTEM

The topology and parameters of the proposed system were based on a reduced equivalent of the AC/DC Itaipu transmission system. The one-line diagram of the system is shown in Figure 1 and its full data are given in Appendix I, so that every result of this paper may be reproduced.

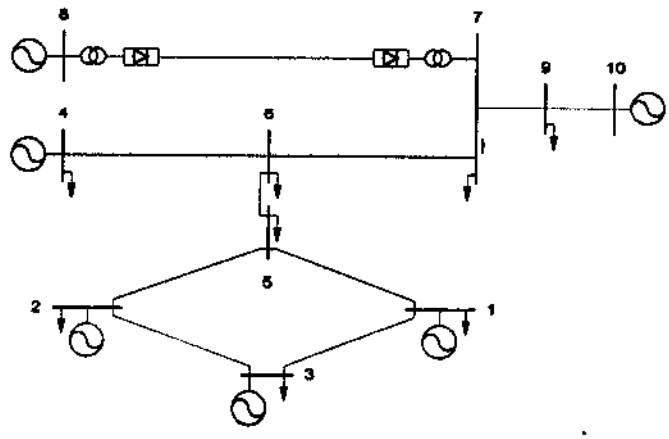

Figure 1. Proposed AC/DC Benchmark System

The machines at buses 4 and 8 respectively represent the Itaipu 60 and 50 Hz generation. The HVDC line and control parameters are very close to the actual values of the Itaipu scheme. Hydro generators at buses 1, 2 and 3 have typical parameters and machine at bus 10 represents a large system equivalent. The system loads were modeled as constant Z, I and P as described in Appendix I.

All generators were modeled as salient pole machines having three rotor windings. The full set of equations used to describe the synchronous generators are given in [5], A simple first-order AVR model, depicted in Figure 2, was made common to all machines. The AVR gains are normally assigned values equal to the ratio $K_a / (2\ T_a)$ [6]. The values used in the benchmark system are lower than that, since this made the studies reported here more attractive.

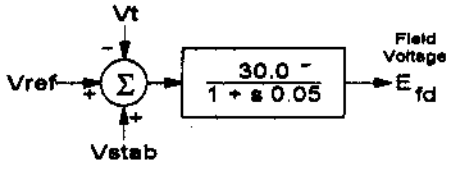

Figure 2. Excitation Control System

The HVDC link modeling is compatible with that described in [7]. The constant gamma control at the inverter station is approximately represented by $\Delta\gamma = 0$. The constant current controller at the rectifier station is represented through the block diagram of Figure 3.

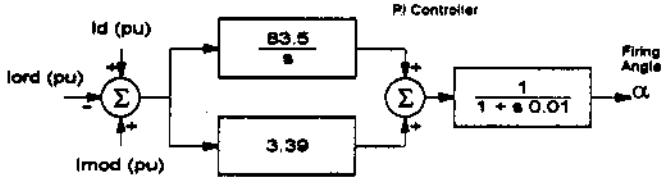

Figure 3. Constant Current Controller at the Rectifier

Consider the operating point described in Table AI-1, the HVDC link operation in constant current control and the loads modeled as described in Table AI-4. This system, in the absence of stabilizing signals, shows an unstable pair of eigenvalues: $\lambda = + 0.450 \pm j\ 3.488$. Table 1 depicts the dominant eigenvalues, their damping factors (ξ) and the dynamic components that contribute most to each oscillatory mode, determined from participation factor information [8].

Eigenvalue	*ξ (%)*	*Maximum Participation Factor*
+0.450 ± j 3.488	- 12.78	Generator 10
- 0.240 ± j 5.605	+ 4.28	Generator 3
- 1.805 ± j 9.195	+ 19.26	Generator 2
- 2.019 ± j 9.173	+ 21.49	Generator 1

Table 1. Dominant System Eigenvalues without Stabilizers

It is highly desirable to have a step response simulation capability in a small-signal stability package, with the ability to display any specified system variable [9,10]. In the comparative analysis of the various stabilization schemes considered in this paper, the step response results are always shown for the same disturbance and set of monitored variables.

Figure 4 shows the step response results for the specified disturbance (+1% at the voltage reference of the excitation control system of generator 4) and the chosen set of monitored variables (voltage magnitude deviations at buses 4, 6, 7 and 8). The unstable mode ($\lambda = +0.450 \pm j\ 3.488$) is quite evident in these plots.

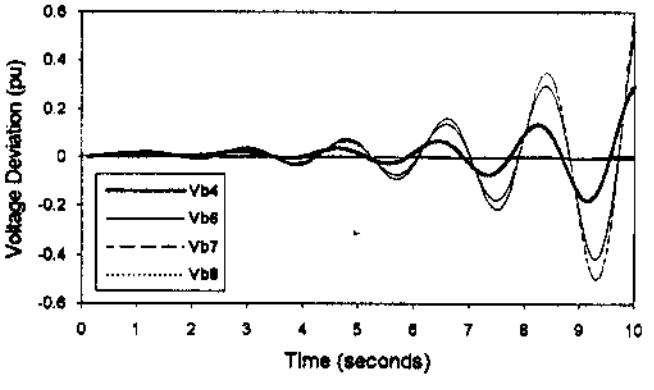

Figure 4. Step Response for the System without Stabilizers ($\lambda = +0.450 \pm j\ 3.488$; $\lambda = -0.240 \pm j\ 5.605$)

Figure 5 shows the mode-shape of rotor speed deviations relative to the unstable mode. The low frequency of oscillation (0.56 Hz or 3.5 rad/s) and the large participation of all system generators are characteristics of an inter-area mode of oscillation. One can note that generators 1, 2 and 3 oscillate in a coherent manner and that generator 8 is the one that oscillates least: the amplitude of its oscillation is only about 2 percent of that of generator 10.

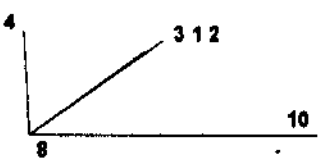

Figure 5. Rotor Speed Mode-Shape for $\lambda = + 0.450 \pm j\ 3.488$

The damping control of this unstable mode can be obtained through the addition of stabilizing signals to the excitation control systems of the generators or to the current controller of the HVDC link. System damping can also be achieved through a Static VAr Compensator properly located in the system and adequately tuned. Another possibility is to employ a FACTS device, such as the advanced series compensator, properly located and tuned, to confer damping to the critical electromechanical mode. All these stabilization options will be investigated in this paper.

Rotor speed mode-shapes and maximum participation factors have been utilized as indicators of the best places in the system for installing power system stabilizers. These two measures will not be used here in favor of more reliable indicators: transfer function residues and transfer function zeros.

3 - CHOICE OF ADEQUATE CONTROL LOOPS AND CONTROLLER DESIGN FOR SYSTEM STABILIZATION

Transfer function residue information can be efficiently calculated and arranged into ranking lists that indicate the most effective dynamic components to damp a particular system mode [11]. The choice of a generator to install a power system stabilizer is based on a ranking list containing the moduli of the residues for the transfer functions $\Delta\omega^i(s)/\Delta V_{ref}^j(s)$, i=1,...,ng (ng being the total number of generators in the system). The generator with the largest modulus of this ranking list is taken as the most adequate for damping the specified mode.

Figures 6, 7 and 8 present, in phasor diagram form, the ranking lists for $\lambda = + 0.450 \pm j\ 3.488$ and transfer functions $\Delta\omega^i(s)/\Delta V_{ref}^j(s)$, $\Delta P_t^i(s)/\Delta V_{ref}^j(s)$ and $\Delta Freq^i(s)/\Delta V_{ref}^j(s)$, i=1,...,ng.

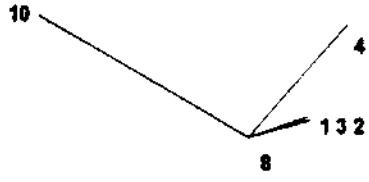

Figure 6. Residues for Transfer Functions $\Delta\omega^i(s)/\Delta V_{ref}^j(s)$ associated with $\lambda = + 0.450 \pm j\ 3.488$

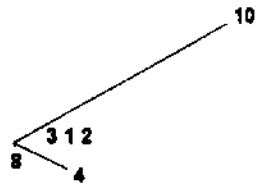

Figure 7. Residues for Transfer Functions $\Delta P_t^i(s)/\Delta V_{ref}^j(s)$ associated with $\lambda = + 0.450 \pm j\ 3.488$

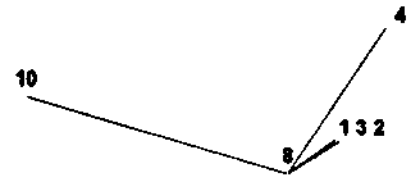

Figure 8. Residues for Transfer Functions $\Delta Freq^i(s)/\Delta V_{ref}^j(s)$ associated with $\lambda = + 0.450 \pm j\ 3.488$

All these ranking diagrams indicate generator 10 and 4 as the two most appropriate to install power system stabilizers to damp the unstable mode. Generator 10 actually represents a whole system area and, therefore, is not considered eligible as a stabilizing source.

The transfer function residues for generator 8 have very low moduli (below 0.1 percent in all the three cases shown). This indicates that a power system stabilizer added to generator 8 is ineffective in damping the unstable mode. This happens mainly because the HVDC link constant current controller would cancel out the electrical power modulation produced by a stabilizer at generator 8. On the other hand, the addition of a stabilizing signal directly to the HVDC link controller is effective in damping this unstable mode, as will be seen in a later section of this paper.

A ranking diagram containing transfer function residue information is of an incremental nature and does not necessarily ensure system stabilization through the closure of any given control loop. The complex plane location of transfer function zeros of a given control loop provides valuable extra information regarding the ease or difficulty with which the system is controlled through this loop [5].

Table 2 presents the critical zeros for various transfer functions considered for stabilization.

Transfer Function	*Critical Zero*
$\Delta\omega^4(s) / \Delta V_{ref}^4(s)$	+ 0.032 ± j 4.812
$\Delta\omega^1(s) / \Delta V_{ref}^1(s)$	+ 0.716 ± j 3.689
$\Delta\omega^2(s) / \Delta V_{ref}^2(s)$	+ 0.650 ± j 3.645
$\Delta\omega^3(s) / \Delta V_{ref}^3(s)$	+ 0.699 ± j 3.693
$\Delta P_t^4(s) / \Delta V_{ref}^4(s)$	+ 0.032 ± j 4.812
$\Delta P_t^4(s) / \Delta I_{ord}^1(s)$	+ 0.259 ± j 3.545
$\Delta V_b^4(s) / \Delta I_{ord}^1(s)$	+ 0.078 ± j 5.097
$\Delta V_b^7(s) / \Delta I_{ord}^1(s)$	+ 0.585 ± j 3.966
$\Delta P_{fs}^{4-6}(s) / \Delta I_{ord}^1(s)$	+ 0.260 ± j 3.541
$\Delta P_{fs}^{6-7}(s) / \Delta I_{ord}^1(s)$	+ 0.297 ± j 3.532
$\Delta Freq^4(s) / \Delta I_{ord}^1(s)$	+ 0.213 ± j 3.576
$\Delta Freq^7(s) / \Delta I_{ord}^1(s)$	+ 0.551 ± j 3.849

Table 2. Critical Zeros for Various Transfer Functions

The effectiveness of a given loop in system stabilization can be properly evaluated through its frequency response analysis, using either Bode or Nyquist plots. This paper deals exclusively with Nyquist plots which are here extensively used for controller design [12].

Figures 9 and 10 show the Nyquist plots of $\Delta\omega^4(s)/\Delta V_{ref}^4(s)$ and $\Delta V_b^4(s)/\Delta I_{ord}(s)$, respectively. Note that the critical zeros of these two transfer functions, according to Table 2, are the least unstable ones. Despite the badly located zeros, a visual analysis of Figure 9 indicates system stabilization to be possible through the addition of a properly tuned stabilizing signal to the excitation control system of generator 4. An analysis of Figure 10 yields the same conclusion regarding the HVDC link controller as a stabilizing source. The design of these stabilizing signals is the object of study in later sections.

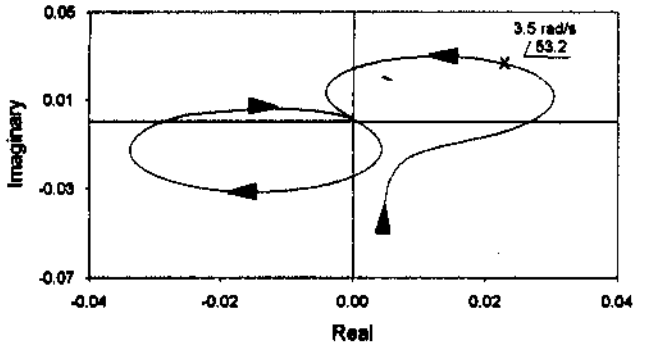

Figure 9. Nyquist Plot of $\Delta\omega^4(s)/\Delta V_{ref}^4(s)$ ($\lambda = +0.450 \pm j3.488$; $Z = +0.032 \pm j4.812$)

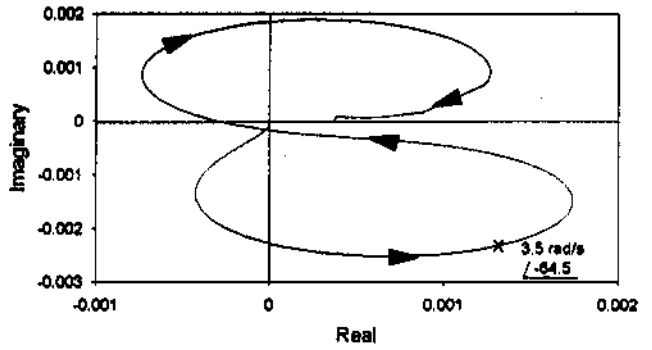

Figure 10. Nyquist Plot of $\Delta V_b^4(s)/\Delta I_{ord}(s)$ ($\lambda = +0.450 \pm j3.488$; $Z = +0.078 \pm j5.097$)

3.1 - System Stabilization through the HVDC Link Controller

In this paper, stabilizer design is carried out utilizing the Nyquist Stability Criterion. A brief description of system stabilization through use of this criterion is presented in Appendix II. Gain and phase compensation are here effected by employing simple lead blocks of the type (1+saT)/(1+sT) tuned as indicated in Appendix II.

The open-loop system has a pair of unstable eigenvalues $\lambda = +0.450 \pm j3.488$, and therefore closed-loop stability is obtained by a counter-clockwise encirclement of the -1 point by the Nyquist plot after compensation. Stabilizer design, based on Figure 10, is obtained by multiplying ΔV_b^4 by a negative gain (to amplify and shift by 180^0 the diagram) and compensate a lag of 65^0 for frequencies about 3.5 rad/s.

Figure 11 shows the block diagram for the HVDC controller stabilizer just designed. A washout block is used to ensure damping action only during transients with no influence on steady-state operation. Figure 12 depicts the Nyquist plot of the open loop transfer function (OLTF) $\Delta I_{mod}(s)/\Delta I_{ord}(s)$, showing the desired counter-clockwise encirclement of the -1 point.

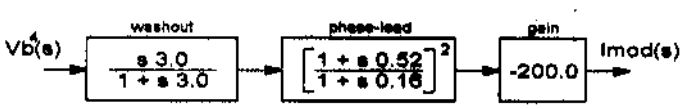

Figure 11. Stabilizing Signal added to the HVDC Constant Current Controller

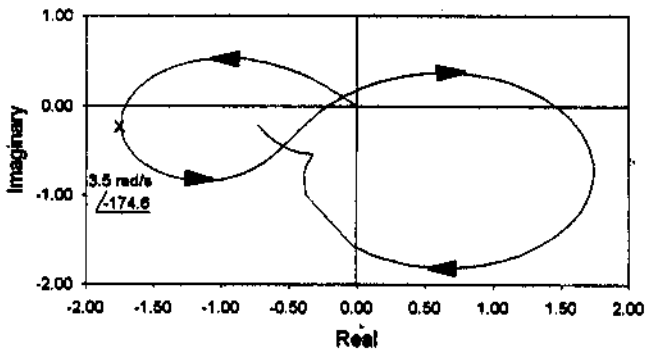

Figure 12. Nyquist Plot of OLTF $\Delta I_{mod}(s)/\Delta I_{ord}(s)$

Table 3 presents the eigenvalues for the stabilized system, where the least damped oscillation has a damping factor (ξ) of about 10 percent.

Eigenvalue	*ξ (%)*	*Maximum Participation Factor*
- 0.323 ± j 3.238	+ 9.93	Generator 10
- 0.531 ± j 4.877	+ 10.83	Generator 10
- 1.800 ± j 9.186	+ 19.23	Generator 2
- 2.007 ± j 9.177	+ 21.37	Generator 1

Table 3. Dominant Eigenvalues for System with HVDC Link Stabilizer

Figure 13 depicts the step response for the system considering the action of the HVDC link stabilizer shown in Figure 11.

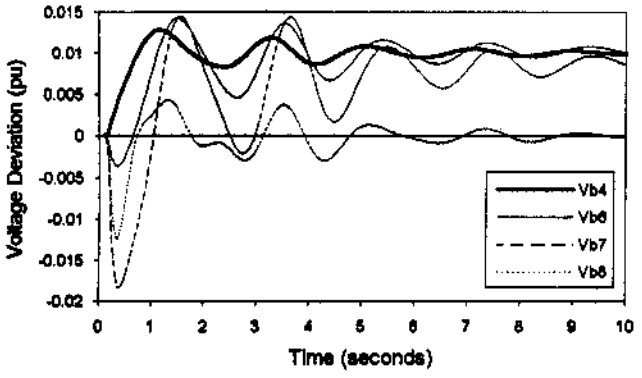

Figure 13. Step Response for System with HVDC Link Stabilizer
(λ = - 0.323 ±j 3.238; λ = - 0.531 ±j 4.877)

3.2 - System Stabilization through a Static VAr Compensator

Static VAr Compensators (SVC) can be effectively used for power system oscillation damping control [13,14]. The definition of SVC location [11], choice of adequate signals and stabilizer design are carried out in this section through the analysis of transfer function residues, transfer function zeros and frequency response plots.

The phasor diagram of Figure 14 shows the residues of the transfer functions $\Delta V_b^i(s)/\Delta B_{var}^i(s)$, i=1,...,nb (nb being the total number of buses in the system) for eigenvalue pair λ= + 0.450 ± j3.488. The symbols ΔV_b^i and ΔB_{var}^i stand for bus voltage and shunt admittance deviations at the i-th bus of the system. This figure shows that bus 6 is the most adequate for installation of a SVC so as to damp the unstable mode.

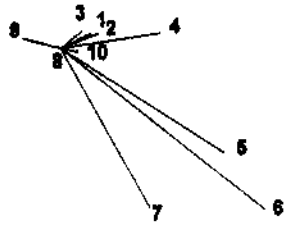

Figure 14. Residues for Transfer Functions $\Delta V_b^i(s)/\Delta B_{var}^i(s)$ associated with λ = + 0.450 ± j 3.488

The installation of a SVC, whose block diagram is shown in Figure 15, yields the dominant eigenvalues depicted in Table 4.

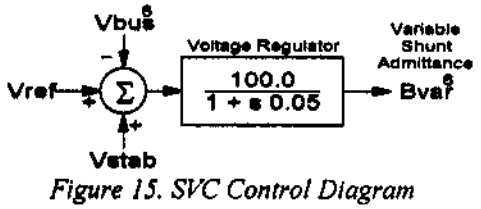

Figure 15. SVC Control Diagram

Eigenvalue	*ξ (%)*	*Maximum Participation Factors*
+0.170 ± j 3.931	- 4.32	Generator 10
- 0.208 ± j 5.649	+ 3.67	Generator 3
- 1.806 ± j 9.169	+ 19.27	Generator 2
- 2.019 ± j 9.173	+ 21.49	Generator 1

Table 4. Dominant Eigenvalues for System with SVC

The installation of a SVC at bus 6, whose controller has the transfer function shown at Figure 15, increased the system synchronizing torques and consequently the frequency of the unstable mode. It, however, did not stabilize the system and therefore it is necessary to include a stabilizing signal to the SVC.

The listing of critical zeros, shown in Table 5, allows the choice of a convenient system variable to be used as an input to the SVC stabilizer. The symbol $V_{ref}^{svc\ 6}$ denotes the voltage reference to the SVC at bus 6.

Transfer Function	*Critical Zero*
$\Delta\omega^4(s) / \Delta V_{ref}^{svc\ 6}(s)$	- 0.354 ± j 5.309
$\Delta\omega^{10}(s) / \Delta V_{ref}^{svc\ 6}(s)$	- 0.313 ± j 5.738
$\Delta Freq^{10}(s) / \Delta V_{ref}^{svc\ 6}(s)$	- 0.376 ± j 7.532
$\Delta Freq^{9}(s) / \Delta V_{ref}^{svc\ 6}(s)$	+ 22.18
$\Delta Freq^{6}(s) / \Delta V_{ref}^{svc\ 6}(s)$	- 0.312 ± j 5.797
$\Delta Freq^{4}(s) / \Delta V_{ref}^{svc\ 6}(s)$	- 0.396 ± j 5.363
$\Delta Freq^{3}(s) / \Delta V_{ref}^{svc\ 6}(s)$	+ 0.383 ± j 6.586
$\Delta P_{fs}^{9-10}(s) / \Delta V_{ref}^{svc\ 6}(s)$	- 0.313 ± j 5.738
$\Delta P_{fs}^{6-7}(s) / \Delta V_{ref}^{svc\ 6}(s)$	- 0.221 ± j 5.810
$\Delta P_{fs}^{7-9}(s) / \Delta V_{ref}^{svc\ 6}(s)$	+ 0.447
$\Delta P_{fs}^{1-3}(s) / \Delta V_{ref}^{svc\ 6}(s)$	+ 0.431 ± j 6.839

Table 5. Transfer Function Critical Zeros to Determine Appropriate Input Signals to the SVC Stabilizer

Many transfer functions have good distribution of zeros in the complex plane, $\Delta Freq^6(s)/\Delta V_{ref}^{svc\ 6}(s)$ included (see Table 6). Variable $\Delta Freq^6(s)$ was chosen as the input to the SVC stabilizer for being a local signal.

Zero	ξ (%)
- 0.312 ± j 5.797	+ 5.37
- 1.784 ± j 9.143	+ 19.16
- 0.832 ± j 4.236	+ 19.27
- 2.264 ± j 10.86	+ 20.41
- 1.988 ± j 9.173	+ 21.19

Table 6. Dominant Zeros of $\Delta Freq^6(s)/\Delta V_{ref}^{svc\ 6}(s)$

The frequency response plot of $\Delta Freq^6(s)/\Delta V_{ref}^{svc\ 6}(s)$ is shown in Figure 16.

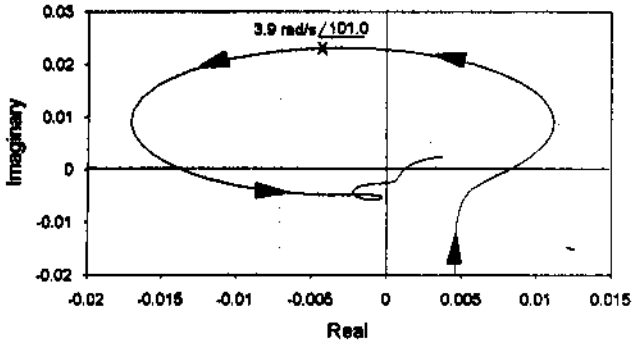

Figure 16. Nyquist Plot of $\Delta Freq^6(s)/\Delta V_{ref}^{svc\ 6}(s)$ (λ=+0.170 ± j 3.931; Z =-0.312 ± j 5.797)

One can note, from Figure 16, that it is necessary to compensate a phase lag of about 80° at frequency 3.9 rad/s and adequately amplify the stabilizing signal. The resulting design is shown in the block diagram of Figure 17. This stabilizing signal turns the system stable as indicated by the Nyquist plot of Figure 18 and by the eigenvalues presented at Table 7. Figure 18 shows that the gain margin is infinite and, therefore, there is no danger of high gain instabilities when using this stabilizing signal. Practical limits to the value of this gain should be determined from non-linear simulations and the use of computer tools which take into consideration the RLC transients of the network.

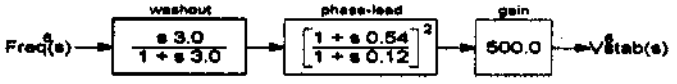

Figure 17. SVC Stabilizing Signal at Bus 6

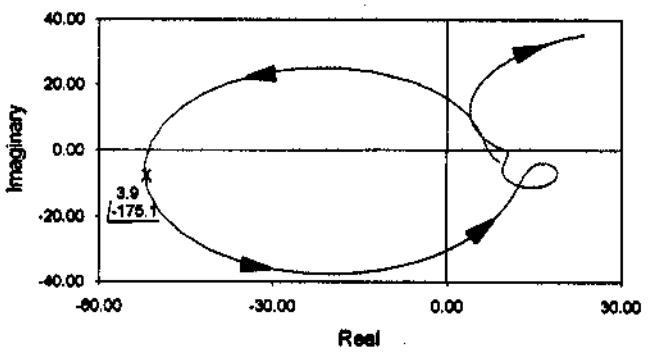

Figure 18. Nyquist Plot of OLTF $\Delta V_{stab}^{6}(s)/\Delta V_{ref}^{svc\ 6}(s)$

Eigenvalue	ξ (%)	Maximum Participation Factor
- 0.302 ± j 5.786	+ 5.20	Generator 3
- 0.793 ± j 4.155	+ 18.75	Generator 10
- 1.790 ± j 9.148	+ 19.21	Generator 2
- 1.991 ± j 9.170	+ 21.22	Generator 1

Table 7. Dominant Eigenvalues with SVC at Bus 6 incorporating a Stabilizing Signal

Figure 19 shows the system time response for the same disturbance and monitored variables as before.

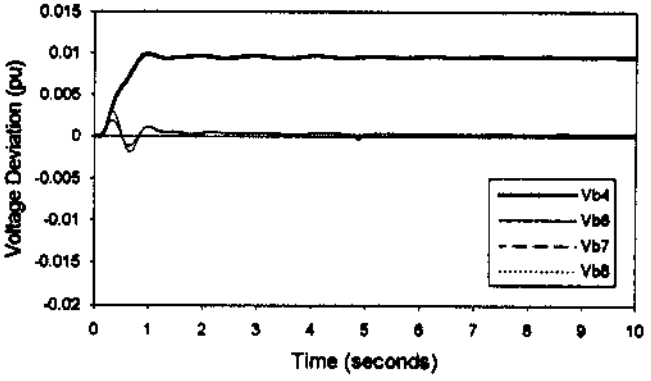

Figure 19. Step Response for System with SVC incorporating a Stabilizing Signal (λ =-0.302 ± j 5.786; λ =-0.793 ± j 4.155)

The use of a SVC or another FACTS device for the sole objective of providing oscillation damping, despite being technically feasible, is economically unacceptable. The cheapest and most effective sources of oscillation damping in practical power systems are the synchronous generators whose excitation control systems incorporate properly tuned stabilizing signals.

In large power systems, for reliability reasons, the task of damping a critical mode of oscillation is not left to a single dynamic component. There are also many cases in which a single stabilizer is not capable of ensuring adequate damping to a given inter-area mode. The reasons above call

for the simultaneous use of various, conveniently located, stabilizers to damp the troublesome modes in the system. An example of a sequential design of multiple stabilizers in the proposed benchmark system is shown in the next section.

3.3 - Optimal Location and Controller Design for FACTS Devices

Figure 20 shows the ranking list, in phasor diagram form, of the major residues for transfer functions $\Delta Pkj^i(s)/\Delta Bkj^i(s)$, i=1,...,nl (nl being the total number of AC lines in the system). The symbol ΔPkj denotes the transit power deviations in the line between buses k and j, while ΔBkj denotes incremental changes in this line susceptance.

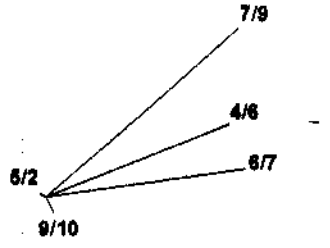

Figure 20. Residues for Transfer Functions $\Delta Pkj^i(s)/\Delta Bkj^i(s)$ associated with $\lambda = +0.450 \pm j\ 3.488$

The residue with the largest magnitude in Figure 20 is associated with the line between buses 7 and 9 pointing this line as the most adequate for installation of an advanced series compensator [15,16]. The second best candidate line is that between buses 6 and 7, which was chosen in the study presented in the next section.

FACTS devices should not be used in radial systems to control line power flow. The authors have obtained results, to be presented in another publication, showing that this control strategy is detrimental to synchronous stability.

The present study considers the use of an advanced series compensator, placed in line 6-7, which only acts as a system oscillation damper. The device controller, shown in Figure 21, was tuned to damp the critical mode ($\lambda = +0.45 \pm j\ 3.488$).

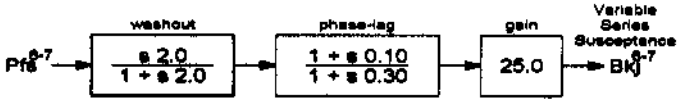

Figure 21. FACTS Device Control Diagram

The eigenvalues shown is Table 8, indicate the high damping action exerted by of the FACTS device, regarding the 3.5 rad/s mode. The other electromechanical mode of 5.3 rad/s becomes, however, very lightly damped. Residue information points generator 3 as the best candidate to stabilize this mode.

Eigenvalue	*ξ (%)*	*Maximum Participation Factor*
- 0.098 ± j 5.359	+ 1.83	Generator 3
- 1.805 ± j 9.195	+ 19.26	Generator 2
- 2.019 ± j 9.173	+ 21.50	Generator 1
- 0.845 ± j 3.238	+ 25.24	Generator 10

Table 8. Dominant Eigenvalues for System with FACTS Device in Line 6-7

The frequency response plot of $\Delta\omega^3(s)/\Delta V_{ref}^3(s)$ is shown in Figure 22. The phase lag of 54° at 5.4 rad/s is properly compensated by the stabilizing signal of Figure 23. This signal turns the system more stable as indicated in the Nyquist plot of Figure 24 and confirmed by the eigenvalues of Table 9. Figure 25 shows the linearized system step response results for the chosen disturbance and monitored variables.

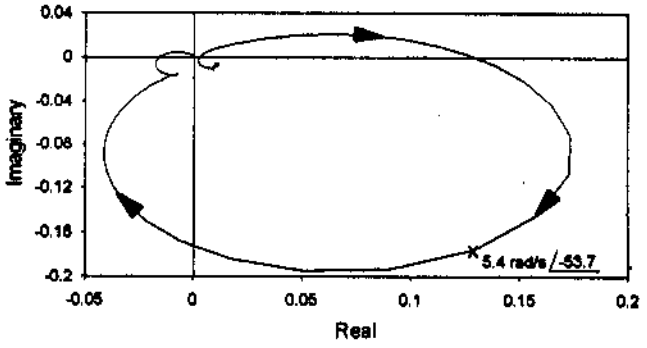

Figure 22. Nyquist Plot of $\Delta\omega^3(s)/\Delta V_{ref}^3(s)$ ($\lambda = -0.098 \pm j\ 5.359$)

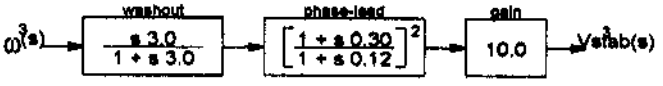

Figure 23. Stabilizing Signal for Generator 3

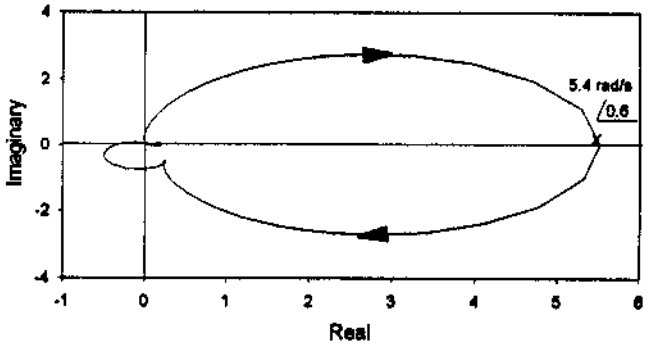

Figure 24. Nyquist Plot of OLTF $\Delta V_{stab}^3(s)/\Delta V_{ref}^3(s)$

Eigenvalue	*ξ (%)*	*Maximum Participation Factor*
- 0.633 ± j 5.331	+ 11.80	Generator 1
- 1.493 ± j 11.00	+ 13.45	Generator 3
- 1.843 ± j 9.205	+ 19.63	Generator 2
- 0.931 ± j 3.476	+ 25.87	Generator 10

Table 9. Eigenvalues for System with FACTS Device in Line 6-7 and Rotor Speed Stabilizer at Generator 3

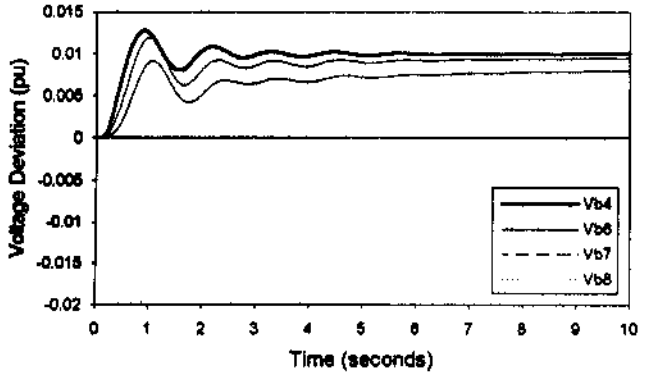

Figure 25. Step Response for System with FACTS Device in Line 6-7 and Rotor Speed Stabilizer at Generator 3

4 - SEQUENTIAL DESIGN OF MULTIPLE STABILIZING LOOPS

The most adequate locations for the stabilizers can be determined from transfer function residue information. Figures 6, 7 and 8 show three phasor diagrams of transfer function residues for $\lambda = +0.450 \pm j\,3.488$. All three diagrams point Generator 4 as the most indicated for the stabilization of the 0.56 Hz mode. Generator 10, the one with the largest residue magnitude, is disregarded for being an equivalent of a whole system area. System stabilization will then be effected through the installation of a stabilizer to the excitation control of Generator 4. Two input signals will be considered: the deviations in rotor speed ($\Delta\omega^4$) and in terminal bus frequency ($\Delta Freq^4$).

The dominant zeros and Nyquist plots of transfer functions $\Delta\omega^4(s)/\Delta V_{ref}^4(s)$ and $\Delta Freq^4(s)/\Delta V_{ref}^4(s)$ are shown in Table 10 and Figures 9 and 26.

$\Delta\omega^4(s)/\Delta V_{ref}^4(s)$	$\Delta Freq^4(s)/\Delta V_{ref}^4(s)$
-	+9.748
+0.032 ± j 4.812	- 0.200 ± j 5.136
- 1.807 ± j 9.187	- 1.805 ± j 9.194
- 2.017 ± j 9.169	- 2.019 ± j 9.173
- 2.757 ± j 4.885	- 1.357 ± j 2.614

Table 10. Dominant Zeros for Transfer Functions $\Delta\omega^4(s)/\Delta V_{ref}^4(s)$ and $\Delta Freq^4(s)/\Delta V_{ref}^4(s)$

The compensated Nyquist plots for both transfer functions are shown in Figures 28 and 29. The same stabilizer parameters, shown in the block diagram of Figure 27, were used in both cases. Note that the terminal bus frequency signal ($\Delta Freq^4$) leads to a very narrow range of gain values for stability being, therefore, inadequate. Problems with the terminal bus frequency signal were previously reported in [12] which showed it to be dynamically active at a higher frequency range than the rotor speed signal.

The adjustment of the gain in the stabilizing loop is made so as to satisfy two constraints: provide the necessary damping to the mode of 3.5 rad/s without pushing the mode of 12 rad/s into the unstable region. These considerations on system conditional stability are made directly from the analysis of the Nyquist plot of Figure 28.

The Root Locus plot of the critical system poles is shown in Figure 30 for a variable gain in the generator stabilizer derived from rotor speed ($\Delta\omega^4$). One can note from both root locus and Nyquist plots that two oscillatory modes become unstable for higher gain values. The first instability occurs at a frequency of 12 rad/s for gain values above 7.5. The second unstable mode occurs at a frequency of 4.8 rad/s for gain values in excess of 60.

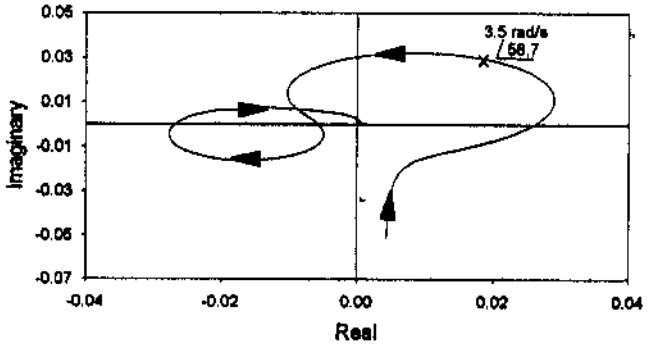

Figure 26. Nyquist Plot of $\Delta Freq^4(s)/\Delta V^4_{ref}(s)$ ($\lambda = +0.450 \pm j3.488$; $Z = +0.032 \pm j4.812$)

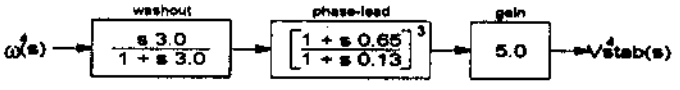

Figure 27. Stabilizing Signal for the Generator at Bus 4

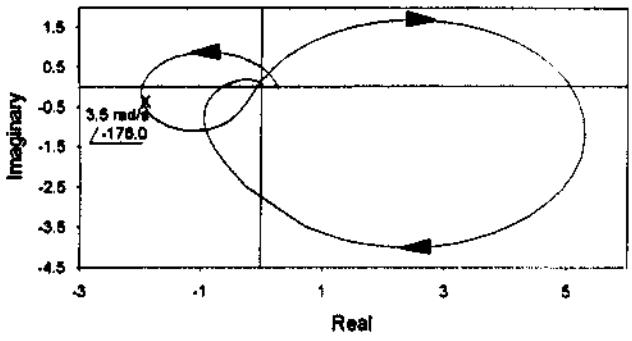

Figure 28. Nyquist Plot of OLTF $\Delta V_{stab}^4(s)/\Delta V_{ref}^4(s)$ for Stabilizer Derived from Rotor Speed

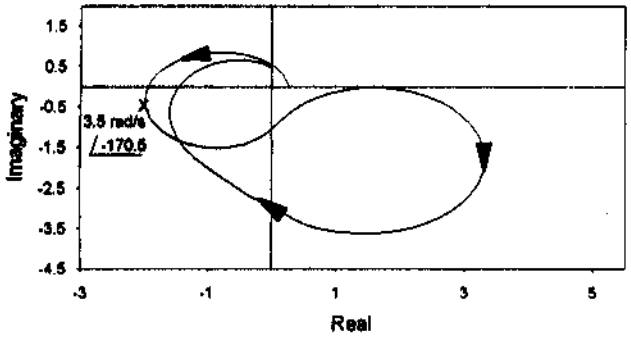

Figure 29. Nyquist Plot of OLTF $\Delta V_{stab}^4(s)/\Delta V_{ref}^4(s)$ for Stabilizer Derived from Bus Frequency

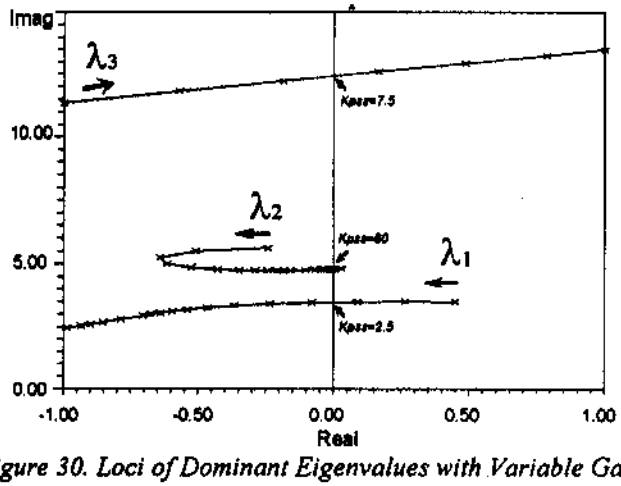

Figure 30. Loci of Dominant Eigenvalues with Variable Gain at Generator 4 Stabilizer

Key: λ_1 - Electromechanical Mode
λ_2 - Electromechanical Mode
λ_3 - Exciter Mode of generator 4

Table 11 contains the dominant eigenvalues for the system with a rotor speed stabilizing signal at generator 4.

Eigenvalue	*ξ (%)*	*Maximum Participation Factor*
- 1.000 ± j 11.34	+ 8.78	Generator 4
- 0.427 ± j 4.780	+ 8.91	Generator 3
- 0.366 ± j 3.324	+ 10.94	Generator 10
- 1.812 ± j 9.182	+ 19.36	Generator 2
- 2.017 ± j 9.166	+ 21.49	Generator 1

Table 11. Dominant Eigenvalues for System with a Rotor Speed Stabilizer at Generator 4

The generator 4 stabilizer damped the critical mode (3.5 rad/s) oscillations up to a certain level. Further damping could not be achieved due to exciter mode instability. The reason for the early instability of the exciter mode is the large phase advance of the stabilizing signal. This, however, was necessary to compensate for the excessive phase lag imposed by the badly located zero (Z =+ 0.032 ± j 4.812) in the $\Delta\omega^4(s)/\Delta V_{ref}^4(s)$ transfer function.

The choice of a second stabilization loop is mandatory to further dampen the critical mode. Figures 31 and 32 show residues of two transfer functions for the critical eigenvalue pair λ =-0.427 ± j 4.780. These residues point generator 3 as the second one to be equipped with a stabilizer.

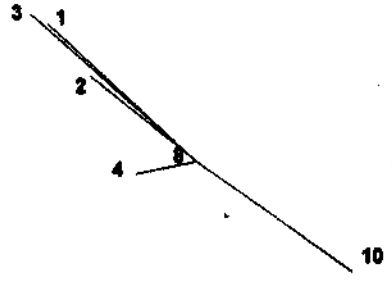

Figure 31. Residues for Transfer Functions $\Delta\omega^i(s)/\Delta V_{ref}^j(s)$ associated with λ = - 0.427 ± j 4.780

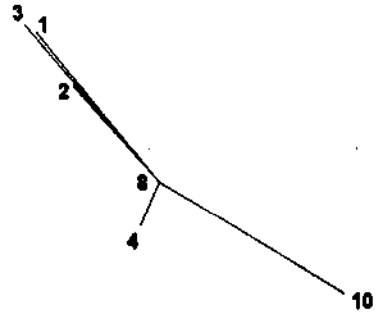

Figure 32. Residues for Transfer Functions $\Delta Freq^i(s)/\Delta V_{ref}^j(s)$ associated with λ = - 0.427 ± j 4.780

The simultaneous closure of two stabilizing loops calls for the analysis of matrix, rather than scalar, transfer function zeros. The transmission zeros concept [5] can be used in this case to verify the ability of these two loops in providing adequate system stabilization.

Table 12 presents the dominant transmission zeros for two (2x2) transfer function matrices.

Transmission Zeros	
$\Delta\omega^4(s)/\Delta V_{ref}^4(s)$ $\Delta\omega^3(s)/\Delta V_{ref}^3(s)$	$\Delta\omega^4(s)/\Delta V_{ref}^4(s)$ $\Delta\omega^2(s)/\Delta V_{ref}^2(s)$
- 1.845 ± j 9.198	-
- 1.259 ± j 5.178	- 0.636 ± j 5.166
- 2.158 ± j 6.308	- 2.019 ± j 9.171

Table 12. Dominant Transmission Zeros for (2x2) Transfer Function Matrices

The stabilizer design for generator 3 is done based on the Nyquist plot of $\Delta\omega^3(s)/\Delta V_{ref}^3(s)$ shown in Figure 33. The open-loop system in this case is already stable and, therefore, to promote greater oscillation damping the Nyquist diagram should be compensated to encircle the +1 point in the clockwise direction, with good gain and phase margins.

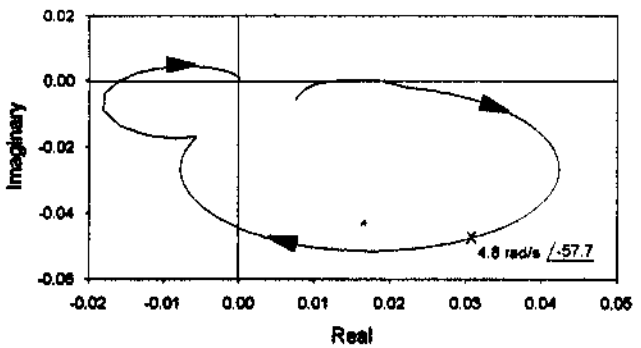

Figure 33. Nyquist Plot of $\Delta\omega^3(s)/\Delta V_{ref}^3(s)$ (λ =-0.427 ±j 4.780)

The calculated stabilizer parameters are depicted in the block diagram of Figure 34. The compensated Nyquist plot $\Delta V_{pss}^3(s)/\Delta V_{ref}^3(s)$ and the associated closed-loop system eigenvalues are shown in Figure 35 and Table 13, respectively.

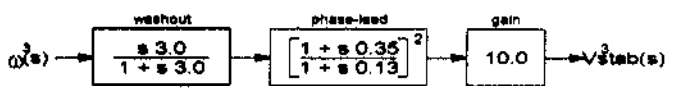

Figure 34. Stabilizing Signal for Generator 3

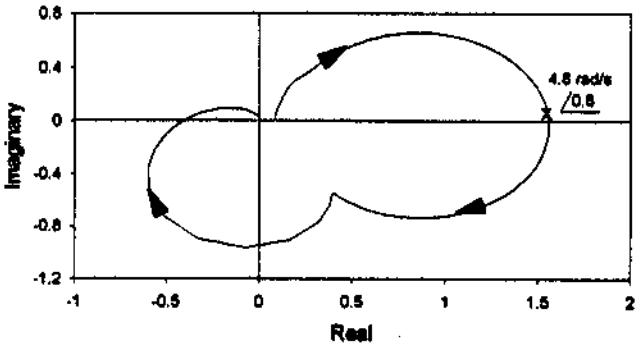

Figure 35. Nyquist Plot of OLTF $\Delta V_{stab}^3(s)/\Delta V_{ref}^3(s)$

Eigenvalue	*ξ (%)*	*Maximum Participation Factor*
- 1.001 ± j 11.28	+ 8.84	Generator 4
- 0.372 ± j 3.314	+ 11.14	Generator 10
- 1.297 ± j 11.36	+ 11.34	Generator 3
- 0.869 ± j 4.673	+ 18.28	Generator 10
- 1.846 ± j 9.200	+ 19.68	Generator 2

Table 13. Dominant System Eigenvalues Generators 4 & 3 with Stabilizers of Figures 27 & 34

Figure 36 displays the step response for the system when having active stabilizers at generators 3 and 4.

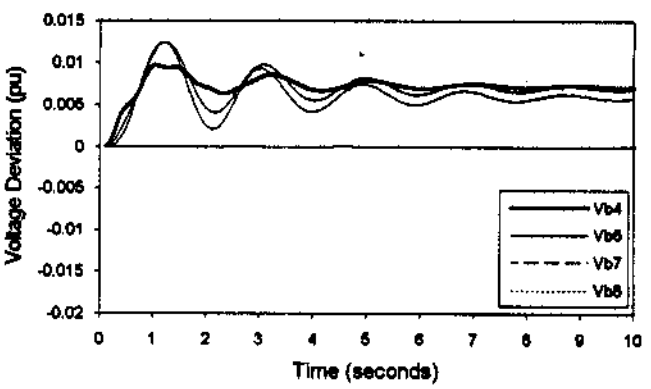

Figure 36. Step Response for System with Active Stabilizers at Generators 3 and 4 (λ =-1. ±j 11.3, λ =-0.37 ±j 3.31)

The choice of a third generator to be equipped with a stabilizer could be effected in the same way as previously described, so as to further damp the 0.5 Hz (ξ=11.14%) mode. In order to give a better tutorial flavour to this exercise the third stabilizer will be added to the HVDC link controller. This exercise is described in the next section.

4.1 - Design of the Third Stabilizing Loop Located at the HVDC Link Controller

The control action of the third stabilizing loop will be exerted by the HVDC current controller. The variable to be used as the input to this stabilizer has not yet been chosen. A pre-selection of best candidate variables can be made based on modal observability analysis. The "mode-shapes" for signals ΔFreq and ΔV_b displayed in Figures 37 and 38, provide the required observability information.

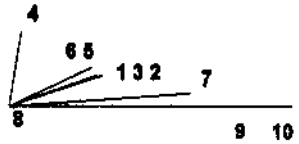

Figure 37. Mode-shape of ΔFreq associated with $\lambda = -0.372 \pm 3.314$

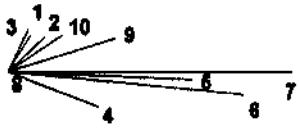

Figure 38. Mode-shape of ΔV_b associated with $\lambda = -0.372 \pm 3.314$

Table 14 contains the dominant transmission zeros for various (3x3) transfer function matrices where only the output of the third loop is varied. The third output of this matrix transfer function corresponds to the HVDC link stabilizer input, which is chosen based on the observability information of Figures 37 and 38.

[F(s)]3x3		*Dominant Transmission*
Input	*Output*	*Zeros*
V_{ref}^4, V_{ref}^3, I_{ord}^1	ω^4, ω^3, $Freq^7$	- 0.813 ± j 5.404 - 1.843 ± j 9.200
V_{ref}^4, V_{ref}^3, I_{ord}^1	ω^4, ω^3, $Freq^9$	- 2.050 ± j 10.36 - 1.845 ± j 9.201
V_{ref}^4, V_{ref}^3, I_{ord}^1	ω^4, ω^3, V_b^4	- 0.467 ± j 3.980 - 1.842 ± j 9.203
V_{ref}^4, V_{ref}^3, I_{ord}^1	ω^4, ω^3, V_b^6	- 0.933 ± j 11.67 - 1.065 ± j 6.121
V_{ref}^4, V_{ref}^3, I_{ord}^1	ω^4, ω^3, V_b^7	+3.783 - 1.844 ± j 9.201

Table 14. Dominant Transmission Zeros for Various (3x3) Transfer Function Matrices

The results of Table 14 indicate that, from the transmission zeros viewpoint, all signals investigated appeared to be adequate (only the ΔV_b^7 signal should be object of some suspicion).

It is good engineering practice to choose local variables as inputs to system controllers. The variable ΔV_b^4 would be chosen on these grounds for being physically close to the HVDC rectifier station. The variable ΔV_b^6 was selected as the stabilizer input based on its better behaved frequency response plot which is shown in Figure 39.

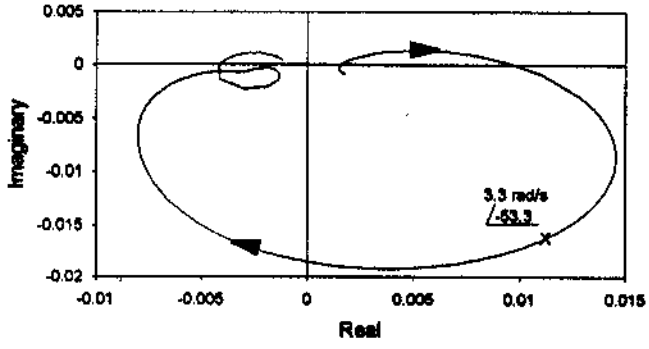

Figure 39. Nyquist plot of $\Delta V_b^6(s)/\Delta I_{ord}^1(s)$ ($\lambda = -0.372 \pm j\ 3.314$)

The properly compensated Nyquist plot and the parameters of the designed stabilizer are shown in Figures 40 and 41.

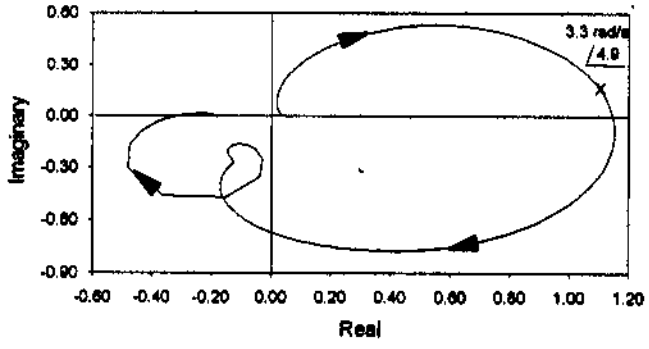

Figure 40. Nyquist plot of OLTF $\Delta I_{mod}(s)/\Delta I_{ord}(s)$

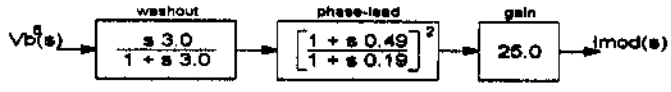

Figure 41. Stabilizing Signal added to the HVDC Current Controller

The dominant system eigenvalues in the presence of these three stabilizers (generators 3 & 4 and HVDC link) are depicted in Table 15. Note that the originally unstable eigenvalue pair ($\lambda = +0.450 \pm j\ 3.488$) is now highly damped ($\lambda = -0.714 \pm j\ 3.037$).

Eigenvalue	*ξ (%)*	*Maximum Participation Factor*
- 0.898 ± j 12.02	+ 7.45	Generator 4
- 1.187 ± j 11.31	+ 10.44	Generator 3
- 0.648 ± j 4.825	+ 13.32	Generator 10
- 1.845 ± j 9.199	+ 19.66	Generator 2
- 0.714 ± j 3.037	+ 22.89	Generator 10

Table 15. Dominant System Eigenvalues in the Presence of Three Stabilizers

The step response of the system in the presence of three stabilizers is shown in Figure 42. The exciter mode of generator 4 (λ=-0.89 ± j 12.0) is excessively present in the terminal voltage dynamic response. The overall design is therefore judged not adequate.

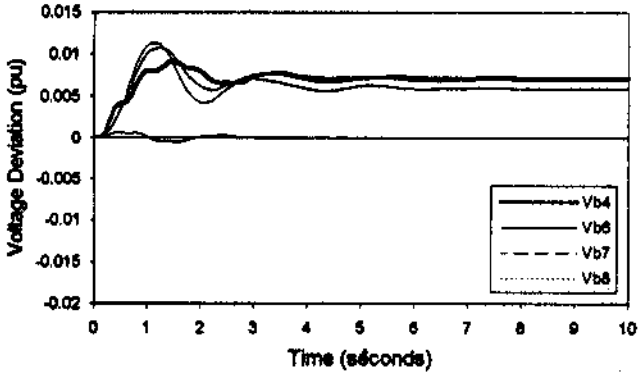

Figure 42. Step Response for System with Three Stabilizers. (λ =-0.89 ±j 12.0, λ =-0.74 ±j 3.03)

A round of sequential retuning was then carried out, one-at-a-time, yielding the revised parameter settings shown in Figure 43.

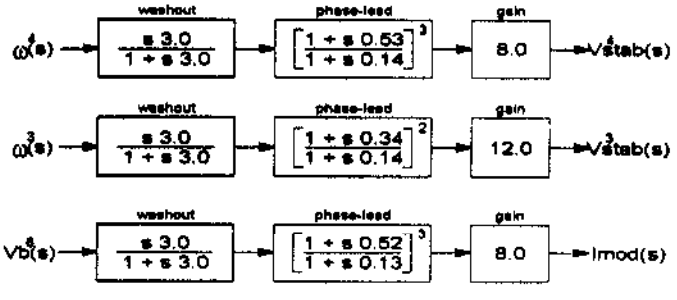

Figure 43. Stabilizer parameters after one-loop-at-a-time retuning

The results obtained, which were quite satisfactory, are shown in Table 16 and Figure 44.

Eigenvalue	*ξ (%)*	*Maximum Participation Factor*
- 1.166 ± j 11.13	+ 10.40	Generator 3
- 0.888 ± j 4.775	+ 18.30	Generator 10
- 0.611 ± j 3.224	+ 18.60	Generator 10
- 1.842 ± j 9.196	+ 19.60	Generator 2
- 2.819 ± j 9.577	+ 28.20	Generator 4

Table 16. System Eigenvalues after one-loop-at-a-time retuning

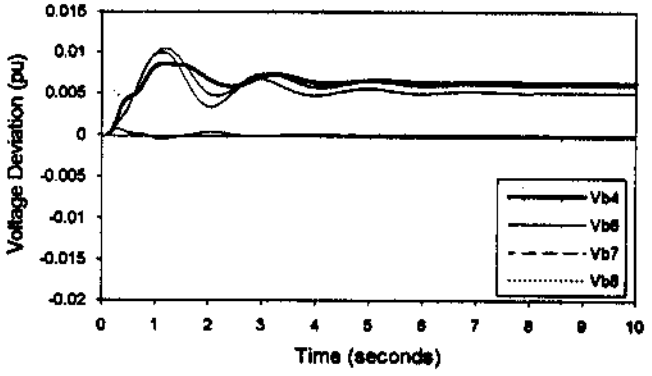

Figure 44. Step Response for System with Three Stabilizers after one-loop-at-a-time retuning

5 - CONCLUSIONS

This paper proposes a small benchmark system for power system oscillation analysis and control. A benchmark system is generally given in the form of a list of data and simulation results. Power system oscillation analysis and control involves the design of various stabilizing loops in an interconnected AC/DC power system.

A decision was made to include not only the list of designed stabilizer parameters, but also describe in detail the adopted stabilizer design procedure. This gave the paper a tutorial nature, which can be useful to those interested in power systems control applications.

The authors have only utilized methodologies and procedures with which they are familiar. There exist other methodologies and procedures for stabilizer tuning in the power system area, but they were not utilized.

The benchmark system here presented will enable power system dynamics engineers to evaluate the performance of their controller design methodologies and software.

The numerous results presented relate to the following aspects:

1- Investigation of small-signal electromechanical stability and control interaction problems.

2- Determination of the most suitable generators in the system for placing power system stabilizers.

3- Determination of the most suitable buses or lines in the system for placing static VAR compensators or advanced series compensators to damp system oscillations.

4- Stabilizer design (generator, SVC, HVDC link, FACTS devices) through frequency response techniques.

5- Choice of control loops and combination of signals best suited for power system stabilization.

6- Time response to a step applied to controller setpoints.

There is no established methodology for the simultaneous design of multiple controllers in large electrical power systems. The conventional single-machine-infinite-bus equivalent has worked well when tuning generator excitation control stabilizers (PSS) in large systems. These stabilizers, in a multimachine environment, usually show robust performance and low dynamic interaction. This is not the case with HVDC links, SVC's or any other FACTS devices, all of which are inertialess equipment with a high speed of response[17].

In a multiple FACTS environment, there may be a high dynamic interaction between these devices and their tuning must therefore be done in a more coordinated manner [18]. Multi-variable frequency response techniques may provide a partial solution to this problem. Multiple pole location techniques also show interesting possibilities.

This paper concludes by stressing the high benefits of having a comprehensive linear analysis package for the study of small-signal electromechanical problems [9,10,19]. A good package should allow the study of large power systems, having a wide variety of components and controller structures, in a CAE environment, where various linear control methods can be used in a complementary manner.

6 - REFERENCES

[1] **CIGRÉ,** "Questionnaire on Electromechanical Oscillations Damping in Power System - Report on the Answer", *ELECTRA*, **no. 64**, pp. 59-70, 1979.

[2] **C. Concordia, Y. Laiho, N. Martins, I. A. Erinmez,** Independent contributions presented at the CIGRÉ 1982 Meeting , in Paris, *Proceedings of CIGRÉ*, **section on System Planning**, pp. 29-36, Paris, 1982.

[3] **V. Arcidiacono, E. Ferrari, R. Marconato, G. Manzoni,** "Problems Posed in Power System Planning by Electromechanical Oscillation Damping and Means for Solution", *International Conference on Large High Voltage Electric Systems (CIGRÉ)*, **paper 31-15**, Paris, Sept. 1982.

[4] **R. T. Byerly, D. E. Sherman, R. J. Bennon,** "Frequency Domain Analysis of Low-Frequency Oscillations in Large Electric Power Systems" *EPRI EL-726 Project RP744-1, Final Report*, Part 1, Palo Alto, CA, April 1978.

[5] **N. Martins & L. T. G. Lima,** "Efficient Methods for Finding Transfer Function Zeros of Power Systems", *IEEE Transactions on Power Systems*, Vol. **PWRS-7**, No. 3, pp. 1350-1361, August 1992.

[6] **De Mello, F. P., Concordia, C.,** "Concepts of Synchronous Machine Stability as Affected by Excitation Control", *IEEE Trans. on Power Aparatus and Systems*, April 1969.

[7] **S. Arabi, G. J. Rogers, D. Y. Wong, P. Kundur, M. G. Lauby,** "Small-Signal Stability Program Analysis of SVC and HVDC in AC Power Systems", *IEEE Transactions on Power Systems*, Vol. **PWRS-6**, No. 3, pp. 1147-1153, August 1991.

[8] **F. L. Pagola, J. J. Pérez-Arriaga, G. C. Verghese,** "On Sensitivities, Residues and Participations. Applications to Oscillatory Stability Analysis and Control", *1988 IEEE Summer Meeting*, paper **88 SM 692-6**, 1988.

[9] **N. Martins, L. T. G. Lima, H. J. C. P. Pinto, N. J. P. Macedo,** "The Brazilian Utilities Package for the Analysis and Control of Small-Signal Stability of Large Scale AC/DC Power Systems", in *Proceedings of III Symposium of Specialists in Electrical Operational and Expansion Planning*, Belo Horizonte, Brazil, May 1992.

[10] **N. Martins, L. T. G. Lima, H. J. C. P. Pinto, N. J. P. Macedo,** "A State-of-the-art Computer Program Package for the Analysis and Control of Small-Signal Stability of Large Scale AC/DC Power Systems", in *Proceedings of IERE Workshop on New Issues in Power System Simulation*, pages 11-19, Caen, France, March 1992.

[11] **N. Martins & L. T. G. Lima,** "Determination of Suitable Locations for Power System Stabilizers and Static Var Compensators for Damping Electromechanical Oscillations in Large Scale Power Systems", *IEEE Transactions on Power Systems*, Vol. **PWRS-5**, pp. 1455-1469, November 1990.

[12] **N. Martins & L. T. G. Lima,** "Eigenvalue and Frequency Domain Analysis of Small-Signal Electromechanical Stability Problems" *IEEE Symposium on Application of Eigenanalysis and Frequency Domain Methods for System Dynamic Performance*, publication **90TH0292-3PWR**, pp. 17-33, 1990.

[13] **A. E. Hammad,** "Application of Static VAr Compensators in Utility Power Systems", *Application of Static VAr Systems for System Dynamic Performance,* **IEEE 87 TH 0187 5 PWR,** pp. 28-35, 1987.

[14] **H. V. Larsen, J. H. Chow,** "SVC Control Design Concepts for System Dynamic Performance", in *IEEE Tutorial Course: Application of SVS for System Dynamic Performance,* publication **87 TH 0187 5 PWR,** pp. 36-53, 1987.

[15] **E. Larsen, C. Bowler, B. Damsky, S. Nilsson,** "Benefits of Thyristor Controlled Series Compensation", *International Conference on Large High Voltage Electric Systems (CIGRÉ),* **paper 14/37/38-04,** Paris, Sept. 1992.

[16] **M. Erche. E. Lerch, D. Povh, R. Mihalic,** "Improvement of Power System Performance Using Power Electronic Equipment", *International Conference on Large High Voltage Electric Systems (CIGRÉ),* paper **14/37/38-02,** Paris, Sept. 1992.

[17] **J. F. Hauer,** "Reactive Power Control as a Means of Enhanced Interarea Damping in the Western U.S. Power System - A Frequency-Domain Perspective Considering Robustness Needs", in *IEEE Tutorial Course: Application of SVS for System Dynamic Performance,* publication **87 TH 0187 5 PWR,** pp. 79-82, 1987.

[18] **N. Martins, N. J. P. Macedo, L. T. G. Lima, H. J. C. P. Pinto,** "Control Strategies for Multiple Static VAr Compensators in Long Distance Voltage Supported Transmission Systems", paper **92 SM 589-2 PWRS** presented at *1992 IEEE/PES Summer Meeting.*

[19] **P. Kundur, G. J. Rogers, D. Y. Wong, L. Wang, M. G. Lauby,** "A Comprehensive Computer Program Package for Small Signal Stability Analysis of Power Systems", *IEEE Trans. on Power Systems,* **PWRS-5,** pp. 1076-1083, 1990.

APPENDIX I: BENCHMARK SYSTEM DATA

System Frequency: 60 Hz; MVA Base: 100 MVA

Table AI-1. Bus Data

Bus	Voltage		Generation	
	Modulus	Angle	MW	MVAr
1	1.030	41.4	1658.0	-363.2
2	1.030	44.1	1332.0	-146.9
3	1.029	43.5	1540.0	-446.6
4	1.039	65.7	6500.0	2200.5
5	0.987	38.1	-	-
6	0.974	38.3	-	-
7	0.941	16.0	-	-
8	1.000	0.0	5200.0	2591.2
9	1.112	-7.1	-	-
10	1.090	0.0	14921.0	-1475.4

Table AI-2.Bus Loadings and Shunt Values

Bus	Load		Shunt
	MW	MVAr	(pu)
1	2405.0	-467.0	1.79
2	692.3	-184.0	1.49
3	688.2	-235.0	1.14
4	62.6	24.3	0.37
5	845.8	-9.2	0.33
6	-4.9	79.8	2.14
7	2884.0	-196.0	2.00
8	-	-	-
9	23000.0	-9000.0	-
10	-	-	-

Table AI-3. Line Data

Line		R	X
From Bus	To Bus	(%)	(%)
1	3	0.030	0.380
2	3	0.050	0.760
4	6	0.029	0.734
5	1	0.190	2.450
5	2	0.150	2.250
6	5	-	0.390
6	7	0.040	0.570
7	9	0.010	0.500
9	10	-	0.100

Table AI-4. Voltage Characteristics of System Loads

Bus	Real Power (MW)		
	% P	% I	% Z
1	-	100.0	-
2	-	100.0	-
3	-	100.0	-
4	-	-	100.0
5	-	-	100.0
6	-	-	100.0
7	-	100.0	-
9	25.0	-	75.0

The MVAr portions of all loads are modeled as 100% constant Z

Table AI-5. Machine Data

Parameter	Generators			
	1 & 2	3	4 & 8	10
MVA	*	1944	6633	20000
T'do (s)	5.00	5.00	7.60	8.00
T"do (s)	0.053	0.06	0.09	0.09
T"qo(s)	0.123	0.09	0.19	0.20
H (kWs/kVA)	4.50	4.50	5.07	5.00
Xd (pu)	0.85	0.88	0.90	1.00
Xq (pu)	0.70	0.69	0.68	0.70
X'd (pu)	0.30	0.30	0.30	0.30
X"d (pu)	0.20	0.20	0.27	0.25
X"q (pu)	0.20	0.20	0.27	0.25

(*) 1900 MVA for Generator 1 and 1400 MVA for Generator 2

Table AI-6. DC Line Parameters

Line		Resistance (%)	Time Constant (s)
From Bus	To Bus		
1	2	4.5571	0.1333

Line resistance calculated for
Vbase = 2400 kV and Ibase = 2610 A

Table AI-7. Converter Station Data

DC Bus	Station	Pdc (MW)	Transf. Tap	Firing Angle (°)
1	Rectifier	5200.0	1.000	15.0
2	Inverter	-5003.3	0.9622	17.0

APPENDIX II

II.1 - The Nyquist Stability Criterion

This section is very brief since this criterion is well discussed in control theory textbooks. The Nyquist criterion allows the assessment of the closed-loop stability of a feedback system from the knowledge of the open-loop transfer function poles and its frequency response plot. Considering the feedback system shown in Figure II.1, the open-loop transfer function (OLTF) is G(s) and the closed loop transfer function is G(s) / (1+G(s)H(s)).

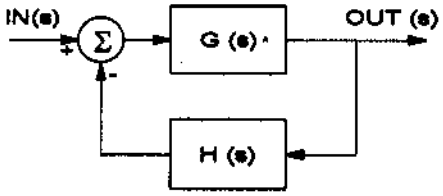

Figure II.1 - Feedback Control System

The Nyquist criterion establishes that: $P_c = P_o + N$, where N is the number of clockwise encirclements of the (-1,0) point of the complex plane made by the frequency response plot of the OLTF as the applied frequency varies from $-\infty$ to $+\infty$. P_o and P_c are the number of unstable poles (eigenvalues) of the open-loop and closed-loop systems respectively. These frequency response plots can be obtained just for positive values of frequencies and in this case they will encircle N/2 times the (-1,0) point of the complex plane. Polar plots or Bode plots can be used to the same effect in this analysis, but the former is preferred by the authors. The terms polar plots and Nyquist plots are used indistinctly in the text.

The design of stabilizing signals applied to generator excitation control systems, static VAr compensators, FACTS devices and HVDC links can be carried out using Nyquist plots. In all cases the power system transfer function is G(s), which can be of high order depending on system size, and H(s) is the transfer function of the stabilizing signal to be designed.

Note: The stabilizing signal is normally considered as a positive feedback (see Figures II.2, II.3, II.4 and II.5) but the Nyquist stability criterion here applied is for the case of a negative feedback. For this reason, all plots shown in the paper were actually multiplied by -1.

II.2 - Stabilizing Signal to the AVR

Figure II.2 shows a block diagram which describes the complete power system dynamics through the AVR control loop. The blocks AVR(s) and PSS(s) correspond to the transfer function of the automatic voltage regulator and the power system stabilizer respectively. The functions $F_1(s)$ and $F_2(s)$ relate the field voltage with the generator terminal voltage and the system variable used as the input to the stabilizer (V_{inp}). The dynamic effects of the generator and the others power system dynamic devices are considered in $F_1(s)$ and $F_2(s)$, which are high order transfer functions. The Nyquist plots shown in this paper are for the condition with the voltage feedback loop (block $F_1(s)$ in Figure II.2) closed.

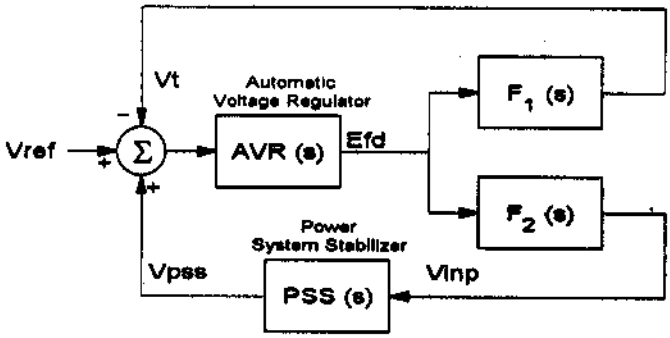

Figure II.2 - Power System Representation Through the AVR Loop

II.3 - Stabilizing Signal to the Static VAr Compensator

Figure II.3 shows a block diagram which describes the complete power system dynamics through the static VAr compensator control loop. The blocks SVC(s) and CSS(s) denote the transfer functions of the static VAr compensator and its stabilizing signal respectively. The blocks $F_3(s)$ and $F_4(s)$ relate the compensator shunt admittance (B_v) with the controlled bus voltage (V_{bus}) and the system variable used as the input to the stabilizer (V_{inp}). The Nyquist plots shown in this paper are for the condition with the voltage feedback loop (block $F_3(s)$ in Figure II.3) closed.

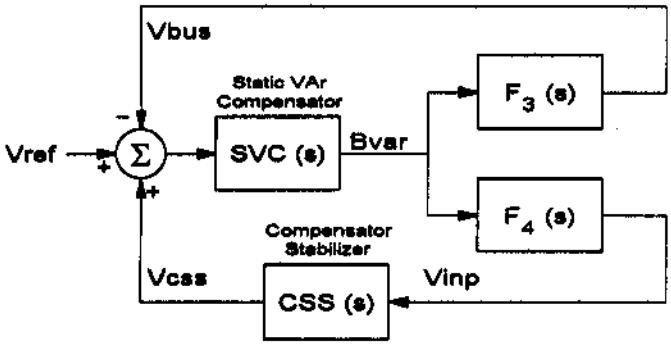

Figure II.3 - Power System Representation Through the Static VAr Compensator

II.4 - Stabilizing Signal to the FACTS Device

Figure II.4 shows a block diagram which describes the complete power system dynamics through the FACTS device control loop. The blocks FACTS(s) and FSS(s) denote the transfer functions of the FACTS device and its stabilizing signal respectively. The blocks $F_5(s)$ and $F_6(s)$ relate the FACTS device output (Out) with the controlled system variable ($V_{controlled}$) and the variable used as the input to the stabilizer (V_{inp}). The FACTS device studied in section 5.1 is not a regulator, but just a power system oscillation stabilizer. In this application, the diagram of Figure II.4 is modified: block $F_5(s)$ does not exist, and the product FACTS(s).FSS(s) is equal to the block diagram of Figure 40.

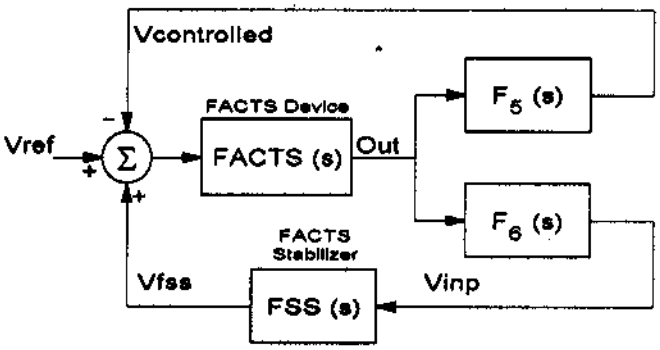

Figure II.4 - Power System Representation Through the FACTS Device

II.5 - Stabilizing Signal to the HVDC Link

Figure II.5 shows a block diagram which describes the complete power system dynamics through the HVDC link control loop. The blocks DCC(s) and DSS(s) denote the transfer functions of the HVDC link and its stabilizing signal respectively. The blocks $F_7(s)$ and $F_8(s)$ relate the HVDC link firing angle (α) with the DC link controlled current (I_{dc}) and the variable used as the input to the stabilizer (V_{inp}). The Nyquist plots shown in this paper are for the condition with the voltage feedback loop (block $F_7(s)$ in Figure II.5) closed.

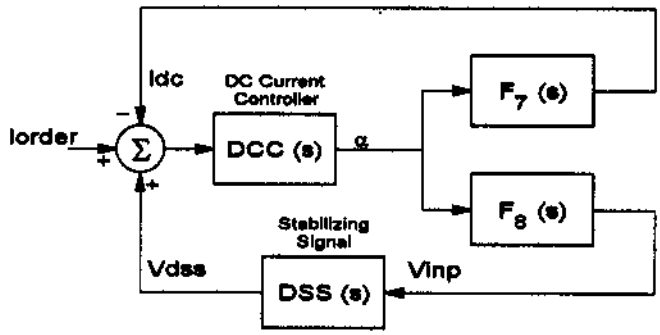

Figure II.5 - Power System Representation Through the HVDC Link

II.6 - Gain and Phase Compensation for Power System Stabilization

The procedure adopted in stabilizer design is to initially deduce compensation circuit parameters only in terms of gain and phase requirements at the frequency, in the Nyquist plot, of the electromechanical mode to be stabilized.

Phase compensation is here effected through the use of one or more phase advance units with transfer function

$$\left(\frac{1+saT}{1+sT}\right) \qquad \text{where } a > 1$$

To minimize high frequency gain, which amplifies the signal noise level and is detrimental to the damping of higher frequency modes, the parameter *a* should be as small as possible. The maximum phase lead angle (ϕ_{max}) obtained with this phase advance unit is given by the expression:

$$\phi_{max} = \sin^{-1}\left(\frac{a-1}{a+1}\right)$$

The time constant *T* determines the frequency ω_{max} at which the maximum phase lead occurs:

$$\omega_{max} = \frac{1}{T\sqrt{a}}$$

The parameter *a* is chosen by making the maximum phase advance equal to the required phase shift at the frequency of the electromechanical mode.